Experimental study of FRP-strengthened concrete beams with corroded reinforcement

Construction and Building Materials 301 (2021) 124076

Contents lists available at ScienceDirect

Construction and Building Materials

journal homepage: www.elsevier.com/locate/conbuildmat

Experimental study of FRP-strengthened concrete beams with corroded reinforcement

Jincheng Yang [a], Reza Haghani [a], Thomas Blanksvärd [b,c], Karin Lundgren [a,*]

[a] Division of Structural Engineering, Department of Architecture and Civil Engineering, Chalmers University of Technology, SE-412 96 Gothenburg, Sweden
[b] Skanska Teknik, Skanska Sverige AB, Warfinges väg 25, SE-112 74 Stockholm, Sweden
[c] Division of Structural and Fire Engineering, Department of Civil, Environmental and Natural Resources Engineering, Luleå University of Technology, SE-971 87 Luleå, Sweden

HIGHLIGHTS

- FRP strengthening method effective for RC beams with severe pitting corrosion.
- CFRP U-jackets instead of repair of deteriorated concrete cover.
- Important to evaluate the local corrosion level.
- Methods to improve the deformation capacity require further studies.

ARTICLE INFO

Article history:
Received 12 February 2021
Received in revised form 8 June 2021
Accepted 22 June 2021

Keywords:
Reinforced concrete
Flexural strengthening
FRP composites
Corrosion-induced cracks
Pitting corrosion
Local corrosion level
3D scanning

ABSTRACT

Corrosion of steel reinforcement is the major cause of deterioration in reinforced concrete structures. Strengthening of concrete structures has been widely studied. However, most research was conducted on sound structures without considering the effects of corrosion. This paper presents an experimental study of the feasibility of using externally bonded FRP laminates combined with U-jackets, applied directly without repairing the deteriorated concrete cover, to strengthen beams with corroded reinforcement. Ten beams were tested in four-point bending. Two beams were not deteriorated and non-strengthened; these served as references. The other eight were pre-loaded to induce flexural cracks and then exposed to accelerated corrosion. Two of the deteriorated beams were not strengthened, three were strengthened with glass-FRP (GFRP) laminates and three with carbon-FRP (CFRP) plates on the beam soffits. On the six strengthened beams, CFRP U-jackets were installed along the span. Local corrosion levels were evaluated with a 3D-scanning technique. Pitting corrosion significantly reduced the load-carrying and deformation capacity of the deteriorated beams. Despite average corrosion levels of 20%, local corrosion levels up to 57% and corrosion-induced cracks up to 1.9 mm wide, the FRP-strengthening method (applied directly to the beams without repairing the deteriorated concrete cover) was effective in upgrading the load-carrying capacity and flexural stiffness. The applied U-jackets effectively suppressed the delamination of the concrete cover and led to the rupture of GFRP laminates and a utilisation ratio of CFRP plates up to 64%. However, improvement in the deformation capacity was not noticeable; this requires further research.

1. Introduction

Numerous civil engineering structures are built of reinforced concrete. Given the enormous investment made in existing structures, their deterioration poses a major challenge for developed countries to ensure the safety of the aging building stock with limited resources. Corrosion of steel reinforcement is the most common cause of deterioration of reinforced concrete [1]. This corrosion affects the structural safety of reinforced concrete structures in several ways. The corroded reinforcement has a reduced effective cross-sectional area and exhibits lower deformability due to notches formed by pitting corrosion [2,3]. Corrosion products generated in the corrosion process also cause a volume expansion, which cracks the concrete cover, undermines the concrete integrity and weakens the bond between reinforcement and concrete. Such corrosion-induced damage significantly impairs the capacity and safety of existing concrete structures. An investiga-

* Corresponding author.
E-mail address: karin.lundgren@chalmers.se (K. Lundgren).

https://doi.org/10.1016/j.conbuildmat.2021.124076
0950-0618/

tion by Mattsson (2008) [4] showed that 72% of the bridges demolished in Sweden during 1990–2005 were torn down due to deterioration and resulting lack of load-bearing capacity. Also other types of structures, such as parking garages and harbours, suffer from deterioration and insufficient load-carrying capacity.

Using bonded fibre reinforced polymer (FRP) composites has been a widely accepted technique for strengthening concrete structures since the pioneering research conducted in the 1980 s [5–7]. FRP composites are characterised by their lightweight, superior strength and high corrosion resistance. Bonded FRP systems are easy to apply on construction sites and effective in improving the serviceability and capacity of concrete structures [8]. Although there has been a vast amount of research into the FRP strengthening of concrete structures over the past four decades, most experimental studies were conducted on sound concrete structures. A few studies were devoted to effective FRP strengthening of deteriorated concrete structures with corroded reinforcement [9,10]. However, in the last 15 years, related research has begun to attract attention [11–22].

Recent literature has clearly shown the importance of considering the effects of corrosion on the structural behaviour of deteriorated concrete structures and the feasibility of applied FRP-strengthening systems. As pointed out by Haddad (2016), corrosion-induced cracks tend to significantly undermine the efficiency of bonded FRP laminates in flexural strengthening. Previous experimental studies [13,23] showed that merely using externally bonded FRP plates could not effectively increase the capacity of concrete beams with corroded reinforcement; the use of bonded FRPs was limited at failure due to separation of concrete cover damaged by corrosion-induced cracks. Besides external bonding, FRP composites are also used as near-surface mounted rods or strips. Before mounting, grooves need to be cut into the concrete cover. However, cutting grooves in corrosion-damaged concrete tends to further undermine the concrete integrity and even cause spalling of the concrete cover. Therefore, previous experimental studies [16,21] on near-surface mounted FRPs to deteriorated concrete beams recommended a patch repair before mounting the FRP, in order to avoid further corrosion, prevent premature separation of concrete cover, and assure a bond between FRP and concrete.

A hybrid configuration of FRP composites (applied in different forms) might be effective in strengthening corrosion-damaged concrete structures. Experimental studies [10,13,21] have shown that using externally bonded FRP laminates combined with FRP wraps/U-jackets may effectively improve the serviceability and load capacity of concrete beams with corroded reinforcement. FRP wraps or U-jackets are commonly used to wrap a concrete member to provide circumferential or transverse confinement. In deteriorated concrete sections, such confinement tends to change the failure mode from concrete cover separation to FRP debonding or rupture, increasing the use of bonded FRP laminates. To optimise the use of U-jackets, those near the end of bonded FRP laminates might be installed at a given angle to provide better anchorage. Fu et al., (2018) [24] investigated the effect of using inclined U-jackets at the ends of bonded FRP laminates and showed that the specimen with 45°-inclined U-jackets exhibited better structural performance than its counterparts with vertically installed U-jackets.

Before bonding FRP laminates to corrosion-damaged concrete members, deteriorated concrete cover was commonly removed through patch repair [15,25,26]. However, a few experimental studies conducted recently [13,27] indicated that, before bonding the FRP laminates, a patch repair to deteriorated concrete cover might not be necessary, given its limited benefits in terms of improving ultimate load and deformation capacity. From the perspective of infrastructure owners, eliminating the need for costly patch repairs is of great interest, especially in refurbishment projects which only require a short-term extension of service life. Therefore, it is necessary to further verify the feasibility of applying the FRP-strengthening system to highly deteriorated but unrepaired concrete cover.

Although the corrosion of steel reinforcement has a significant impact on the structural behaviour of deteriorated concrete beams and the efficiency of FRP strengthening [10,27], existing literature on the FRP-strengthening of deteriorated concrete beams (to the authors' knowledge) merely evaluates the reinforcement corrosion damage in terms of average corrosion level (in other words, steel mass loss as a percentage). However, using the average corrosion level fails to represent local corrosion damage due to pitting corrosion and tends to overestimate the capacity of deteriorated structures. Therefore, it is of great importance to have a good knowledge of the local corrosion level (cross-sectional area loss as a percentage) along the reinforcement.

In the current study, an experimental programme was conducted to investigate the efficiency of FRP-strengthening methods in deteriorated reinforced concrete beams with corroded steel reinforcement. The FRP-strengthening system was applied directly, without repairing the corrosion-damaged concrete cover. Corrosion of steel reinforcement was evaluated by both average corrosion and maximum corrosion levels, using a 3D optical scanning technique. The FRP-strengthening efficiency was estimated based on the flexural behaviour of beam specimens subjected to four-point bending tests to failure.

2. Experimental programme

As shown in Table 1, the test programme included ten beams categorised into four groups: RN, DN, DG, and DC. The first group (RN) included two sound beams as references. The other eight beams were, after three-week-curing, subjected to three-point bending to induce pre-cracks and then exposed to identical conditions of accelerated corrosion for 75 days. The pre-cracking and accelerated corrosion were designed to induce a combination of pitting and general corrosion in tensile reinforcement, considered an proper representation of the practical corrosion problems [28]. After the corrosion period, the two beams in group DN were not strengthened, the three beams in group DG were flexurally strengthened with GFRP laminates bonded to the beam soffits, and the three beams in group DC were bonded with CFRP plates. CFRP U-jackets were installed in the six strengthened beams, to provide transverse confinement and anchorage to the bonded GFRP laminate or CFRP plate. All specimens were subjected to four-point bending tests until failure to investigate their flexural behaviour. After these tests, the tensile reinforcement was removed from the deteriorated beams to measure the corrosion levels. Further details of the experimental programme are described in the following sections.

2.1. Reinforced concrete beams

Fig. 1 shows the dimensions of the beams and the position of steel reinforcement. Each beam was reinforced with two ribbed Φ12 bars in the tension zone and two ribbed Φ10 bars in the compression zone. Stirrups (ribbed, Φ8) were placed at a spacing of 125 mm with clear concrete cover of 20 mm, whereas no stirrups were placed in the mid-600 mm region of the beams. All stirrups were wrapped in two layers of PVC electrical insulation tape (0.15-mm-thick per layer) from the bottom to half their height. The PVC-wrapping was used to insulate the stirrups from tensile reinforcement to be connected to impressed current for accelerated corrosion. The insulation assured a well-defined exposure area of steel rebars to artificial electrochemical corrosion, based

Table 1
Test programme.

Specimen[a]	Flexural strengthening material	Average corrosion level[b] [%]		Max. local corrosion level[c] [%]	
		I[d]	II[d]	I	II
RN1	–	–		–	
RN2	–	–		–	
DN1	–	20	19	50	48
DN2	–	20	21	46	54
DG1	GFRP	22	17	51	40
DG2	GFRP	21	20	43	54
DG3	GFRP	18	23	43	53
DC1	CFRP	23	20	53	55
DC2	CFRP	21	22	49	41
DC3	CFRP	21	22	54	57

[a] The first letter refers to reference (R) or deteriorated (D); the second letter refers to non-strengthened (N), strengthened with GFRP laminate (G), or strengthened with CFRP plate (C).
[b] Average corrosion level means the percentage of the mass loss of reinforcement over the corroded length.
[c] Maximum local corrosion level refers to the maximum percentage of the cross-sectional area loss along a steel reinforcement bar.
[d] Corrosion levels are reported separately for the two tensile reinforcement bars, I and II, in each of the beam specimens.

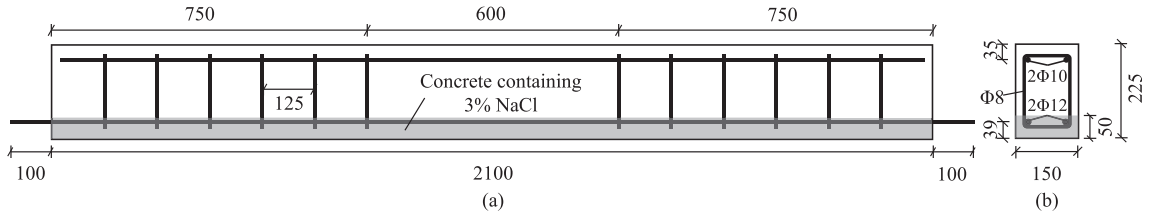

Fig. 1. Dimensions and cross-section of the ten reinforced concrete beams cast in the laboratory (unit: mm).

on which the magnitude of the impressed current was determined, to obtain expected corrosion level of tensile rebars over a certain period. Ready-mix concrete was used to cast the ten beams in the laboratory. NaCl (3.0% of the weight of cement) was added to the concrete mix in the lower 50 mm to reduce the electrical resistance of the concrete cover and thus shorten the corrosion initiation time. After casting, the beams were covered with polyethylene sheets and cured in an indoor climate (20±2°C, 60±10% RH).

2.2. Pre-cracking

After three weeks of curing, the eight beams in groups DN, DG, and DC were subjected to three-point bending with an effective span of 1.8 m and pre-loaded to 25.2 kN. The maximum pre-load was equivalent to 60% of the theoretical yielding load [20,29], representing a reasonable load level in serviceability limit state. The pre-loading induced pre-cracks to provoke pitting corrosion in the subsequent accelerated corrosion period. At the maximum pre-load, five to six cracks occurred in the mid-region of the beams. At loading, the maximum crack width close to the midspan, at the height of tensile reinforcement, was in the range of 0.08 to 0.16 mm, whereas the crack widths outside the mid-400 mm region were smaller than 0.08 mm. However, once the load was removed, crack widths in the mid-400 mm region decreased significantly. All crack widths on the bottom surfaces of the eight beams were between 0.03 and 0.08 mm, as measured one day after pre-cracking.

2.3. Accelerated corrosion

The pre-cracked beams were exposed to accelerated corrosion, using an impressed current on the reinforcement to obtain an average corrosion level of 20%. To avoid any negative effects of a high corrosion rate [30], a constant impressed current of 150 mA was used, corresponding to a current density of 220 μA/cm^2 over the corroding area of the tensile reinforcement bars. As a comparison, the current density in most recent studies is commonly chosen in the range of 100 to 500 μA/cm^2 [13,19,20,30,31,32].

To ensure constant current during the corrosion period, an electrical circuit was set up for each beam with an independent channel of power supply, see Fig. 2. Corrosion of the tensile reinforcement not only undermines the flexural behaviour of RC beams due to the reduced cross-sectional area of steel bars, but also weakens the bond between the steel bars and surrounding concrete and can thus induce anchorage problem at the ends of tensile rebars. As the flexural behaviour was the focus of the current study, the corrosion was designed to occur mainly in the mid-region of the tensile rebars, to avoid corrosion-induced anchorage problems at their ends. As shown in Fig. 2, a plastic container was placed under the supported beam. On the lateral sides, the container was cut to accommodate the beam. Gaps between beam and container were carefully sealed with a waterproof sealant. After 24-hour-curing, an electrolyte solution of 3.5% NaCl was poured into the container to the level of the tensile reinforcement. A stainless-steel wire mesh (approx. 600 × 200 mm^2) was placed in the NaCl solution below the beam soffit and connected to the power supply, serving as the cathode. The tensile bars extending 100 mm out of the beam were charged with constant current, serving as the anode. During the corrosion period, water was added to the NaCl solution every two days to compensate for evaporation loss and keep the solution level at the designed height.

2.4. FRP-strengthening method

After the accelerated corrosion phase, the six deteriorated beam specimens in groups DG and DC were strengthened with FRP composites. The FRP-strengthening procedure mainly included: 1) the pre-treatment of concrete surfaces and corners, 2) bonding GFRP

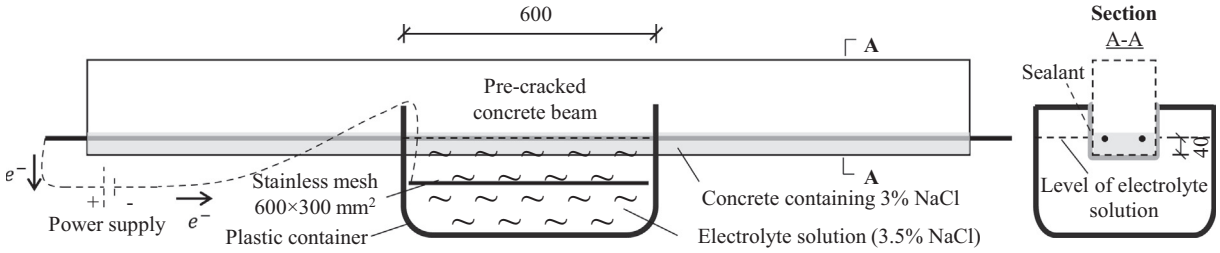

Fig. 2. Electrical circuit set-up for the accelerated corrosion of pre-cracked concrete beams and side view of the beam in the plastic container.

laminates or CFRP plates onto the beam soffits for flexural strengthening, and 3) installing CFRP U-jackets for transverse confinement.

The pre-treatment was conducted in accordance with EN1504-10 [33] to coarsen concrete surfaces before bonding and prepare round cross-section corners for U-jacket installation. After cleaning, the concrete surfaces were coated with a thin layer of epoxy primer (StoPox 452 EP) to seal voids on the surfaces and avoid trapping air during the subsequent FRP bonding step.

Fig. 3 shows the schematic for bonding FRP composites. In group DG, a GFRP laminate was applied to the beam soffit with the wet layup method - nine layers of E-glass fibre fabrics were impregnated in epoxy-based resin (StoPox LH) and then stacked to form the laminate. The glass fibre fabric was cut into strips 1500 mm long and 150 mm wide; 68% of the fibres were placed in the longitudinal (span) direction and 32% transversely. In group DC, a 1.5-meter-long CFRP plate was bonded to individual beam soffits using epoxy adhesive. The CFRP plate was a pultruded FRP product with unidirectional carbon fibres (StoFRP Plate IM 100C); the plate cross-section was 100 × 1.45 mm^2. The adhesive was a two-component epoxy (StoPox SK41); the thickness of the adhesive layer was 2 mm.

After 48-hour curing of the bonded GFRP/CFRP, U-jackets were installed in groups DG and DC. The U-jackets were made of unidirectional carbon fibre fabrics (StoFRP Sheet IMS300-C300) impregnated in epoxy resin (StoPox LH) and bonded to the beams with the wet layup method. One layer of the carbon fibre fabric was used for the vertically installed U-jackets, whereas three layers were stacked up for the four 45°-inclined U-jackets. The bonded FRP system was cured for four weeks (minimum seven days required) before the structural failure tests.

2.5. Material properties

The mix proportions of concrete by weight were cement:sand:gravel:water = 1:2.46:1.90:0.43. Based on standard compressive tests of concrete cubes (side length 150 mm) following EN 12390–3:2019 [34], the average compressive strength of the concrete cubes was measured as 68.2 MPa (CoV 5.7%) at 28 days and 78.7 MPa (CoV 5.0%) on the day of the structural failure test. According to standard tests of concrete cylinders (100 mm diameter and 200 mm height) following EN 12390–13:2013 [35], the elastic modulus of concrete on the day of testing was 33.3 GPa (CoV 7.7%). The fracture energy of concrete was estimated at 134 N/m on the day of testing, based on wedge-splitting tests using the configuration described in Lövgren et al., [36]. The steel reinforcement used in all beams was B500C hot-rolled ribbed bars. Based on the standard tensile test of reinforcement according to ASTM A615 [37], the mean values of mechanical properties are listed in Table 2.

The FRP composites used in the present study included GFRP laminates, CFRP plates, and CFRP U-jackets. Eight dog-bone samples were prepared when applying the GFRP laminates and CFRP U-jackets using the wet layup method. Standard tensile tests were conducted in accordance with ASTM D638-14 [38] to measure the elastic modulus and ultimate strain at rupture, see Table 3. The elastic moduli of GFRP laminates and CFRP U-jackets in Table 3 are reported together with their cross-sectional dimensions, considering the fact that the measured elastic modulus of laminates is a result of not only the type of fiber sheets/fabrics but also the amount of epoxy matrix applied during the wet layup procedure. It should also be noted that the U-jacket dog-bone samples used three layers of carbon fibre fabric; the same as the inclined end U-jackets shown in Fig. 3. For the vertical U-jackets using only one layer of fabric, while their thickness was 1/3 that of the tested samples, their mechanical properties may be assumed to be the same. Material properties of the pultruded CFRP plate were measured in a previous study [39], based on standard tensile tests following ASTM D3039 [40]. The epoxy adhesive (StoPox SK41) between the CFRP plate and concrete had an elastic modulus of 7.1 GPa and tensile strength of 34 MPa after 14-day curing at room temperature [41].

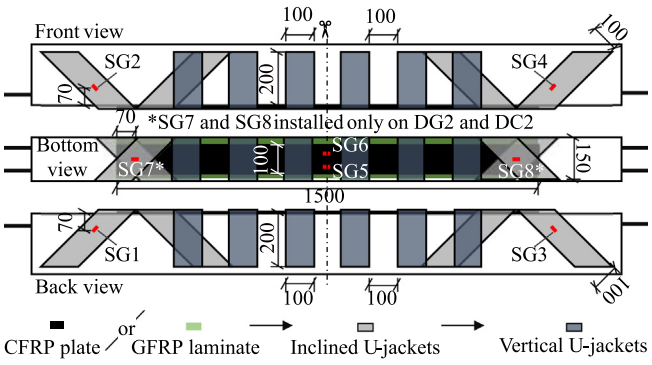

Fig. 3. Schematic of FRP composites applied to deteriorated concrete beams in groups DG and DC, including the position of strain gauges (SG1-SG8).

2.6. Structural tests to failure

All specimens were eventually subjected to structural testing until failure to investigate their flexural behaviours and failure modes. Fig. 4 shows the test set-up for the specimens in four-point bending. The specimens were simply supported on two movable steel supports, providing an effective span of 1.8 m. A distribution beam was used, between the specimen and a hydraulic cylinder, to achieve symmetrical loading and create a 600 mm span of constant moment in the specimen. External load from the hydraulic cylinder was applied in a displacement-controlled manner; the displacement rate imposed on the distribution beam was 1.0 mm/min. For the reference specimens in group RN, the displacement rate was increased to 3.0 mm/min after yielding of the tensile reinforcement.

During the tests, net-deflection at midspan was monitored using three linear, variable differential transformers (LVDT) placed

Table 2
Material properties of steel reinforcement.

Steel reinforcement	E_s [GPa]	f_{sy} [MPa]	f_{su} [MPa]	ε_{su} [%]
Tensile bars Φ12	191	570	661	8.1
Compressive bars Φ10	200	528	630	8.9
Stirrups Φ8	202	531	654	9.6

Notations: E_s—elastic modulus;f_{sy}—yield strength; f_{su}—ultimate tensile strength; ε_{su}—ultimate tensile strain.

Table 3
Material properties of FRP composites.

Sample of FRP composites	Width × Thickness[1] [mm × mm]	E_f [GPa]	ε_{fu} [%]
GFRP laminate	12.8 × 3.03	20.2	1.82
CFRP U-jacket[2]	12.8 × 2.39	57.6	1.24
CFRP plate	25.0 × 1.45	214	1.27

Notations: E_f—elastic modulus; ε_{fu}—ultimate tensile strain at rupture; [1]Width and thickness of tested samples. For GFRP and U-jackets, the width refers to the narrow section of dog-bone coupons; [2]U-jacket samples used three layers of carbon fibre fabrics same as the inclined U-jackets.

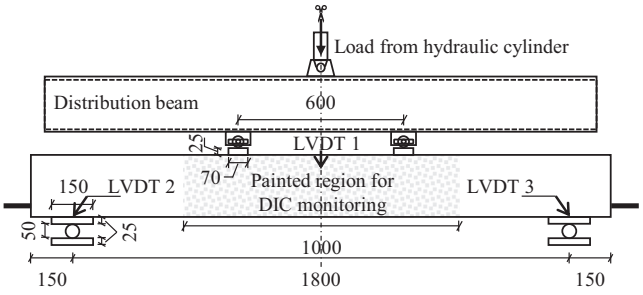

Fig. 4. Test set-up of structural testing to failure in four-point bending.

at the midspan section and centre of the two steel supports. The axial strains in the FRP composites were measured with strain gauges (SG1-SG8) installed at critical positions, see Fig. 3. The digital image correlation (DIC) technique was used to monitor the side face of beam specimens within the mid-1000 mm zone. The monitored region was first painted in white and then black paint was applied with a sponge to generate a random and evenly distributed pattern of black dots. An ARAMIS® adjustable stereo camera system [42] was used to acquire geometrical data by taking images at a frequency of 1 Hz. The collected geometrical data was subsequently processed in software GOM® Correlate [43] to monitor and visualise the deformation field and cracking on the monitored surface.

2.7. Evaluation of corrosion level

After the structural failure tests, the corroded rebars were taken out and cleaned in a sandblasting cabinet to remove surface rust. The sandblast cleaning used silica sand under 5–7 bar of pressure [44]. The average and local corrosion levels were evaluated for each corroded rebar, based on the loss of mass and local cross-sectional area respectively.

The weight of the corroded bars was measured after sandblasting and compared with the initial weight, documented before casting the beams. The corrosion outside the mid-900 mm length of the rebars was negligible (see Section 3.1). Thus, the average corrosion level of each rebar in this zone was estimated as:

$$\mu_{avg} = \frac{m_{loss}/900}{m_{bar}/2300}, \tag{1}$$

where m_{loss} is the mass loss of the corroded bar and m_{bar} is the mean mass (1991 g; CoV = 0.19%) of the twenty 2300 mm-long tensile bars used in the specimens.

To evaluate the local corrosion level along the tensile bars, a 3D optical scanning technique was used to investigate their local cross-sectional area. After sandblasting, geometrical data on the corroded bars was collected using a 3D scanner at an accuracy of 0.1 mm and then compared with the initial data collected before casting. The geometrical data was compared, to analyse the loss of cross-sectional area along the bar length. The maximum local corrosion level was then calculated as:

$$\mu_{max} = \max\left(\frac{A_0(x) - A_{fin}(x) - \Delta A_{yn}(x)}{A_0(x)}\right), \tag{2}$$

where $A_0(x)$ is the initial cross-sectional area along the bar length x, documented before beam casting, $A_{fin}(x)$ is the final cross-sectional area along the bar length x, evaluated after the structural failure test, and $\Delta A_{yn}(x)$ refers to the decrease of cross-section area caused by yielding and necking of the tensile bar. The effect of yielding and necking is challenging to estimate, as discussed in Section 3.2.

3. Corrosion damage on specimens

3.1. Corrosion-induced cracks

The patterns and widths of the corrosion-induced cracks in the eight deteriorated beams (groups DN, DG, and DC) were documented after the corrosion phase. These documented crack patterns showed that the corrosion-induced cracks propagated beyond the submerged section and developed more or less within the mid-900 mm region. Along each tensile bar, at least one corrosion-induced crack was observed on the bottom surface or/and side of the beam. The width of the corrosion-induced cracks was measured in seven sections at a spacing of 150 mm, see Fig. 5. In some sections along bars DG3-II, DC3-I, and DC3-II, two corrosion-induced cracks occurred on the bottom surface and side of the beams; the measured widths of these two cracks were added

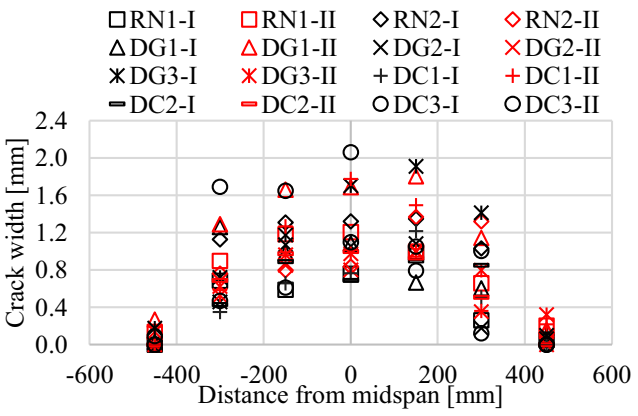

Fig. 5. Width of corrosion-induced cracks measured every 150 mm along all sixteen tensile bars in eight deteriorated beams.

up for the section and plotted in Fig. 5. Although the crack width measurements were widely dispersed, the mean values indicated that the corrosion-induced cracks were wider nearer the midspan. The crack widths at the midspan were in the range of 0.7 to 1.9 mm.

3.2. Corrosion level

The average and maximum corrosion levels, μ_{avg} and μ_{max}, of each tensile reinforcement bar are listed in Table 1. The mean value of μ_{avg} was 20.5%, reasonably close to the designed average corrosion level of 20%. The maximum local corrosion level μ_{max} was much higher, ranging from 40 to 57% with a mean value of 49.3%. Therefore, the average corrosion level could not be used to represent damage caused by pitting corrosion.

Fig. 6(a and c) shows the initial (A_0) and final (A_{fin}) cross-sectional areas of the two tensile bars in specimen DG1 as examples. At any cross-section, the difference between A_0 and A_{fin} includes the area reduction due to corrosion, general yielding, and local necking, as stated in Eq.2.

The effect of yielding was investigated by examining the distance between ribs in the initial and final states of bars close to the ruptured section. No obvious changes in the rib distance were observed. The limited yielding effect might be explained by the fact that: 1) the deteriorated specimens failed at relatively small midspan deflections and the uniform strain in the tensile reinforcement was below 1% in theoretical calculations and 2) tensile deformation of corroded reinforcement tended to localise in critical sections with deep corrosion pits, instead of exhibiting uniform elongation. Accordingly, it was concluded that the effect of yielding on the cross-section reduction could be assumed negligible in this study.

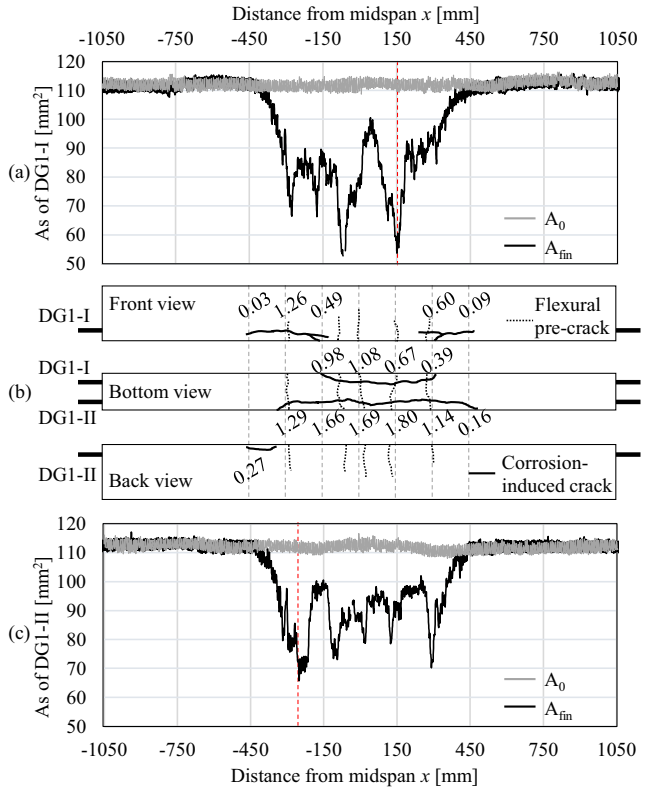

Fig. 6. (a, c) Cross-sectional areas of the tensile reinforcement bars I and II in specimen DG1; (b) flexural pre-cracks and corrosion-induced cracks measured every 150 mm (unit in mm).

However, the local necking effect in the ruptured section was significant. Fig. 7 shows the bar segments near the rupture section of DG1-I. Given the missing geometrical information at the rupture section, it was difficult to quantify the local necking effect on the reduced cross-sectional area. As a simplification, the critical necking region was assumed to take place between two peak-area points closest to the rupture section. The cross-sectional area between these two peak points was assumed to be linear before the development of necking, see Fig. 7.

4. Results and discussion of structural tests

4.1. Flexural behaviour

The flexural behaviour of all tested specimens is presented in Fig. 8, in terms of load–deflection curves. In general, the experimental results showed good consistency in each group regarding the flexural behaviour and failure mode. The two reference beams, RN1 and RN2, reached the ultimate stage at a maximum load of approx. 80 kN; the subsequent flexural failure was initiated by concrete crushing on the compressive side of the beams, see Fig. 9(a). The flexural response of the deteriorated beams DN1 and DN2 was seriously affected by the corroded reinforcement. These beams failed due to rupturing of the corroded tensile reinforcement, accompanied by concrete cover spalling/delamination

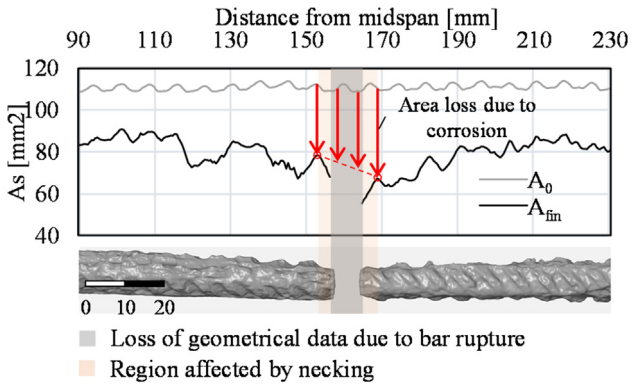

Fig. 7. Assumptions to calculate the cross-sectional loss due to corrosion at the rupture section of bar DN2-I.

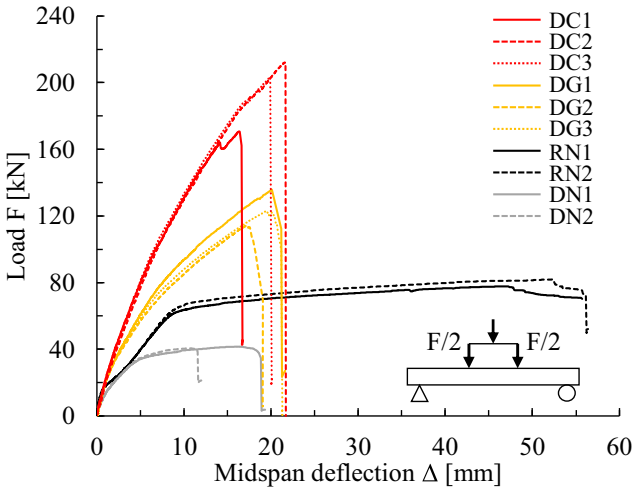

Fig. 8. Load-deflection curves of all ten specimens subjected to four-point bending in the structural failure tests.

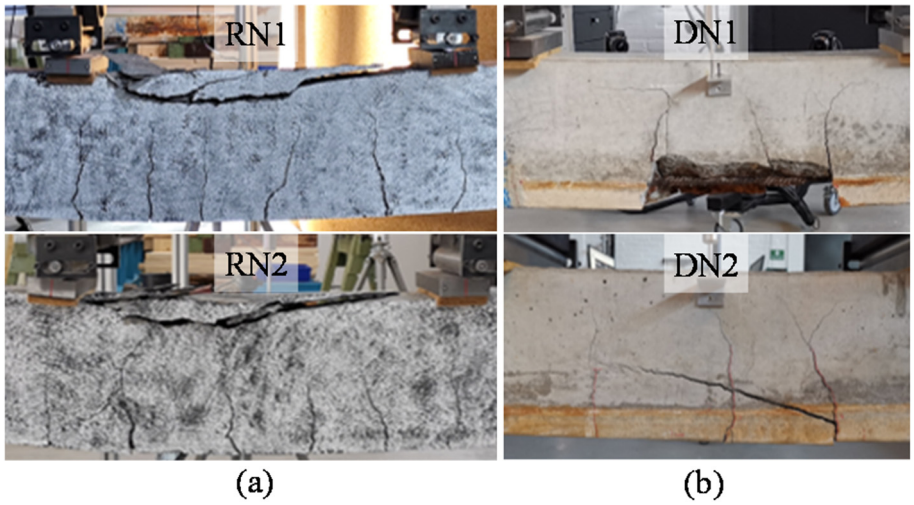

Fig. 9. Flexural failure due to: (a) concrete crushing in the reference beams RN1 and RN2 and (b) rupture of corroded tensile reinforcement bars, accompanied by concrete cover spalling off in DN 1 and concrete cover delamination in DN2.

Table 4
Ultimate capacity and failure mode of all specimens in the structural failure tests.

Specimens	F_u [1] [kN]	Δ_u [1] [mm]	Failure mode
RN1	77.7	46.7	CC[2]
RN2	81.9	52.3	CC
DN1	41.5	16.3	RS[3]
DN2	40.6	10.7	RS
DG1	135.8	20.1	RG[4]
DG2	114.4	17.3	RG
DG3	123.0	19.5	RG
DC1	170.8	16.4	AC[5]
DC2	212.2	21.6	AC
DC3	203.3	19.9	AC

[1] F_u and Δ_u = maximum load and corresponding midspan deflection in the ultimate state; [2]CC = concrete crushing on the compression side of the beam; [3]RS = rupture of tensile rebars; [4]RG = rupture of GFRP laminate; [5]AC = anchorage failure at end of CFRP plate.

on the tensile side of the beam, see Fig. 9(b). The FRP strengthening of the deteriorated beams in groups DG and DC significantly increased the flexural stiffness and ultimate load-carrying capacity. At the maximum load, brittle failure took place; rupture of GFRP laminates in group DG and anchorage failure of CFRP laminates in group DC. The ultimate capacity and failure mode of each specimen are summarised in Table 4.

4.2. Effects of corroded steel reinforcement

Compared to the reference group, the deteriorated beams in group DN showed significant reductions in flexural stiffness, load-carrying capacity, and deformation capacity at failure, owing to the reduced effective area and ductility of highly corroded tensile reinforcement. For instance, specimens DN1 and DN2 reached the maximum load of 41.5 kN and 40.6 kN; 48% and 49% lower than the ultimate capacity of the reference beams (79.8 kN on average). The reduced ultimate load capacity in group DN agreed well with the maximum local corrosion levels of the tensile reinforcement bars, in the range of 46% to 54%, see Table 1. Obviously, using the average corrosion level would overestimate the yield and ultimate load-carrying capacity of the deteriorated beams in the current study.

The high local corrosion level (due to pitting corrosion) not only reduces the cross-sectional area but also greatly impairs the ultimate strain of the corroded tensile bars [3]. As a result, the flexural failure of specimens DN1 and DN2 was governed by reinforcement rupturing at a much smaller midspan deflection than that of the reference specimens. The difference in deformation capacity between DN1 and DN2 shows the sensitivity to local corrosion levels: DN1 rebars had 50% and 48%, while DN2 rebars had 46% and 54% (Table 1). At the ultimate state of DN1, both rebars ruptured and the load dropped to almost zero, while for DN2, merely the rebar with the larger maximum local corrosion level ruptured; this took place at a smaller deformation compared to DN1.

4.3. Use of bonded FRP for flexural strengthening

The load–deflection curves in Fig. 8 show that the hybrid configuration of bonded FRP composites effectively improves the flexural stiffness and load-carrying capacity of the deteriorated beams in groups DG and DC. After the FRP-strengthening, the maximum loads increased up to 136 kN in group DG and 212 kN in group DC, which was 70% and 165% higher than the average load capacity of the reference group. The great improvement in flexural responses was attributed to good utilisation of the bonded GFRP laminate or CFRP plate for flexural strengthening.

Fig. 10 (a) shows the development of tensile strains on the GFRP laminate, measured at the midspan. In group DG, rupture of the bonded GFRP laminate was observed at the failure of the specimens. Fig. 10(b) shows the ruptured GFRP laminate in specimen DG1 as an example. In group DC, the failure of the specimens was initiated by the anchorage failure of the CFRP plate from one of the ends, see Fig. 11(b). The brittle anchorage failure was accompanied by substantial energy release, which subsequently caused debonding/rupture of U-jackets and concrete cover delamination in local regions. Fig. 11(a) shows the tensile strains measured at the midspan section of the CFRP plate. At the moment of failure, the tensile strain at midspan reached as high as 0.81% in DC2, equivalent to a utilisation ratio of 64%.

Although the applied FRP strengthening significantly upgraded the load capacity of the deteriorated beams, no improvement in ultimate deformation (compared to the unstrengthened specimen DN1) was noticeable.

4.4. Confinement with U-jackets

In most applications of CFRP as externally bonded reinforcement, only 20–30% of the strength of CFRP may be utilised [45].

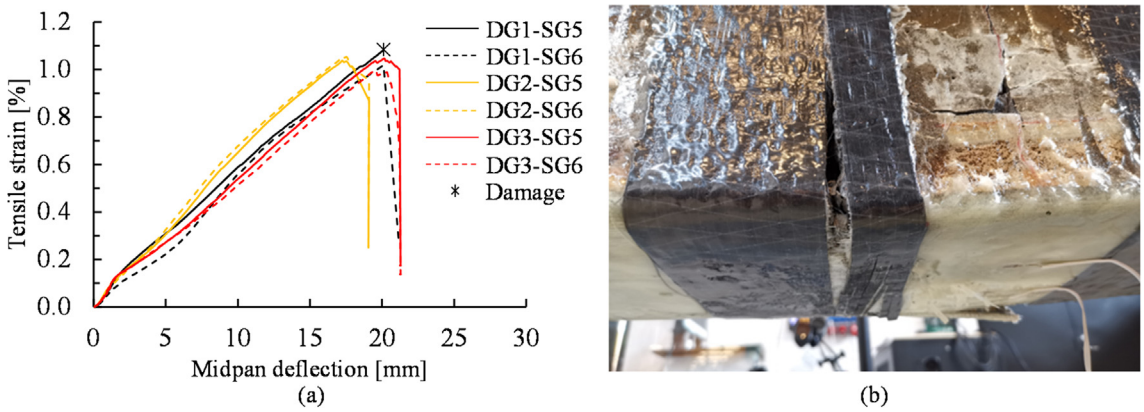

Fig. 10. (a) Tensile strains measured by SG5 and SG6 at the midspan of the GFRP laminates; (b) failure of specimen DG1 due to rupture of the GFRP laminate close to midspan.

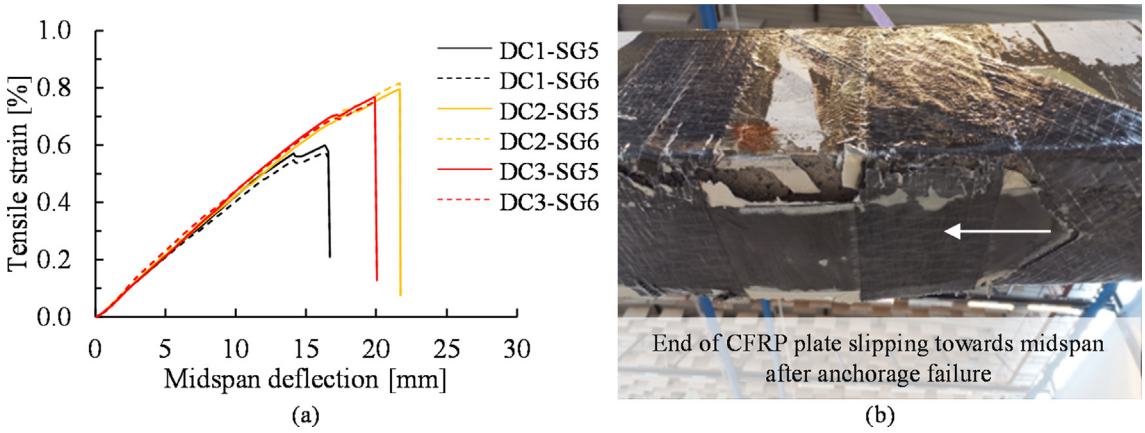

Fig. 11. (a) Tensile strains measured by SG5 and SG6 at the midspan of the CFRP laminates; (b) anchorage failure of the CFRP plate in specimen DC1.

In the current study, even though the FRP was bonded to deteriorated concrete cover involving corrosion-induced cracks with widths of up to 1.9 mm, the utilisation ratio of the bonded CFRP reached 64% in group DC and GFRP laminates were ruptured in group DG. The high utilisation of bonded FRP was attributed to the transverse confinement provided by the U-jackets.

In the deteriorated beams, the confinement offered by the U-jackets was able to limit the opening of corroded-induced cracks, suppress the delamination of deteriorated concrete cover, and postpone the debonding of the GFRP laminate/CFRP plate. The U-jackets effectively prevented the delamination of the deteriorated concrete cover until failure of the bonded FRP in groups DG and DC. Fig. 12 compares cracking propagated in the constant-moment region of specimens DN2, DG2, and DC2 at the same midspan deflection; the cracks were highlighted in the maximum principal strain field monitored by DIC. The comparison showed that the U-jackets installed in specimens DG2 and DC2 effectively suppressed the initiation of concrete cover delamination observed in the deteriorated but unstrengthened specimen DN2. Note that DN2 even had a much smaller load in this comparison, as the deflection was kept constant.

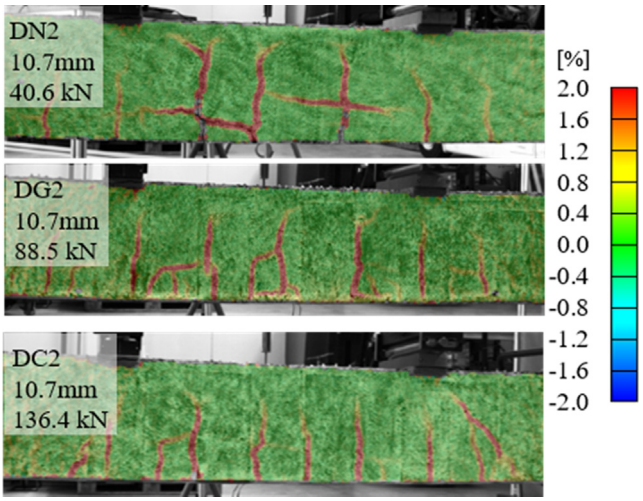

Fig. 12. Comparison of cracks on the side of specimens (DN2, DG2, and DC2), visualised in the maximum principal strain field monitored by DIC at the same midspan deflection of 10.7 mm.

5. Conclusions

The current experimental study investigated the feasibility of using externally bonded FRP laminates combined with U-jackets for flexural strengthening of deteriorated concrete beams with highly corroded steel reinforcement. The FRP-strengthening system was applied to the beams without repairing the deteriorated concrete cover. The efficiency of the FRP-strengthening method was evaluated based on the flexural behaviour of the specimens subjected to four-point bending tests to failure. Based on the experimental results, the following conclusions were drawn:

- The combined use of externally bonded FRP on beam soffits and CFRP U-jackets along the span was efficient in upgrading the load-carrying capacity of deteriorated concrete beams, even though maximum local corrosion levels of the reinforcement were up to 57%. For example, after strengthening, the ultimate load capacity of the deteriorated specimen DC2 increased to 212 kN, which was 417% and 165% higher, respectively, than that of deteriorated non-strengthened specimens and the reference beams.
- The FRP-strengthening method was effective, even though it was applied directly to the beams without repairing the deteriorated concrete cover. Given that the maximum width of corrosion-induced cracks was up to 1.9 mm on the deteriorated concrete cover, the applied U-jackets effectively suppressed the delamination of the concrete cover and led to the rupture of GFRP laminates and a utilisation ratio of CFRP plates up to 64%. Compared to the utilisation of 20–30% in most applications of externally bonded CFRP [45], the current strengthening efficiency was satisfactory.
- The flexural responses of tested specimens showed the importance of evaluating the local corrosion level of steel reinforcement in accurately estimating the flexural capacity of deteriorated concrete beams. For instance, compared to that of the reference beams, the ultimate load of deteriorated beam DN1 was reduced by 48%. This reduction agrees well with the maximum local corrosion levels of 50% and 48% in the two tensile reinforcement bars of specimen DN1. Instead, using the average corrosion level in DN1 (20% and 19% as shown in Table 1) would overestimate its flexural capacity.
- Although the applied FRP-strengthening method significantly upgraded the load-carrying capacity of the deteriorated concrete beams, the deformation capacity was not noticeably improved.

Further studies are needed to investigate possible solutions to improve the deformation capacity of deteriorated reinforced concrete structures. Although the U-jackets efficiently confined and suppressed the delamination of concrete cover in the tested beams, the confinement efficiency of U-jackets may decrease with increased beam widths. The effects of beam width on the efficiency of applied U-jackets are suggested to be studied further. For the practical maintenance and inspection of existing concrete structures, there is great demand for non-destructive techniques to efficiently detect and monitor the local corrosion level of embedded steel reinforcement. Future research is also required to establish design methods to provide practical guidance on the FRP strengthening of deteriorated concrete structures with corroded steel reinforcement.

CRediT authorship contribution statement

Jincheng Yang: Conceptualization, Methodology, Software, Validation, Formal analysis, Investigation, Data curation, Writing - original draft, Visualization. **Reza Haghani:** Conceptualization, Methodology, Validation, Writing - review & editing, Supervision. **Thomas Blanksvärd:** Conceptualization, Methodology, Validation, Writing - review & editing, Supervision. **Karin Lundgren:** Conceptualization, Methodology, Validation, Writing - review & editing, Supervision, Project administration, Funding acquisition.

Declaration of Competing Interest

The authors declare that they have no known competing financial interests or personal relationships that could have appeared to influence the work reported in this paper.

Acknowledgements

This work was financially supported by the Swedish Transport Administration [grant number BBT-2018-011]. CFRP composites were donated by Sto Scandinavia AB. Special thanks to Dr. E Chen and Dr. Carlos Gil Berrocal for their help with test design and data processing.

References

[1] K. Gkoumas, F. Marques Dos Santos, M. van Balen, A. Tsakalidis, A. Ortega Hortelano, M. Grosso, A. Haq, F. Pekar, Research and innovation in bridge maintenance, inspection and monitoring - A European perspective based on the Transport Research and Innovation Monitoring and Information System (TRIMIS), 2019, doi:10.2760/719505 (accessed December 6, 2020).
[2] I. Fernandez, J.M. Bairán, A.R. Marí, Corrosion effects on the mechanical properties of reinforcing steel bars. Fatigue and σ–ε behavior, Constr. Build. Mater. 101 (2015) 772–783, https://doi.org/10.1016/j.conbuildmat.2015.10.139.
[3] E. Chen, C.G. Berrocal, I. Fernandez, I. Löfgren, K. Lundgren, Assessment of the mechanical behaviour of reinforcement bars with localised pitting corrosion by digital image correlation, Eng. Struct. 219 (2020), https://doi.org/10.1016/j.engstruct.2020.110936.
[4] H.-Å. Mattsson, Integrated bridge maintenance : evaluation of a pilot project and future perspectives, PhD dissertation, KTH, 2008, http://urn.kb.se/resolve?urn=urn:nbn:se:kth:diva-9572 (accessed November 15, 2020).
[5] H. Katsumata, Y. Kobatake, T. Takeda, A study on the strengthening with carbon fiber for earthquake-resistant capacity of existing reinforced concrete columns, in: Proceedings of 9th World Conference on Earthquake Engineering, Tokyo-Kyoto, Japen, 1988: pp. 518–522.
[6] T.C. Triantafillou, N. Deskovic, Innovative prestressing with FRP sheets: mechanics of short-term behavior, J. Eng. Mech. 117 (1991) 1652–1672, https://doi.org/10.1061/(ASCE)0733-9399(1991)117:7(1652).
[7] U. Meier, Rehabilitation and retrofitting of existing structures through external bonding of thin carbon fibre sheets, Mater. Struct. 28 (1995) 105–106, https://doi.org/10.1007/BF02473179.
[8] L.C. Hollaway, A review of the present and future utilisation of FRP composites in the civil infrastructure with reference to their important in-service properties, Constr. Build. Mater. 24 (2010) 2419–2445, https://doi.org/10.1016/j.conbuildmat.2010.04.062.
[9] J.F. Bonacci, M. Maalej, Externally bonded fiber-reinforced polymer for rehabilitation of corrosion damaged concrete beams, SJ. 97 , 2000, 703–711, https://doi.org/10.14359/8805.
[10] E.M. Tamer, S. Khaled, Carbon-fiber-reinforced polymer repair to extend service life of corroded reinforced concrete beams, Journal of Composites for Construction, 9, 2005, 187–194, https://doi.org/10.1061/(ASCE)1090-0268(2005)9:2(187).
[11] O. Benjeddou, M.B. Ouezdou, A. Bedday, Damaged RC beams repaired by bonding of CFRP laminates, Constr. Build. Mater. 21 (2007) 1301–1310, https://doi.org/10.1016/j.conbuildmat.2006.01.008.
[12] M. Bergström, Assessment of existing concrete bridges: bending stiffness as a performance indicator, 2009.
[13] A.H. Al-Saidy, K.S. Al-Jabri, Effect of damaged concrete cover on the behavior of corroded concrete beams repaired with CFRP sheets, Compos. Struct. 93 (2011) 1775–1786, https://doi.org/10.1016/j.compstruct.2011.01.011.
[14] M.M. Fayyadh, H. Abdul Razak, Assessment of effectiveness of CFRP repaired RC beams under different damage levels based on flexural stiffness, Constr. Build. Mater. 37 (2012) 125–134, https://doi.org/10.1016/j.conbuildmat.2012.07.021.
[15] J. Xie, R. Hu, Experimental study on rehabilitation of corrosion-damaged reinforced concrete beams with carbon fiber reinforced polymer, Constr. Build. Mater. 38 (2013) 708–716, https://doi.org/10.1016/j.conbuildmat.2012.09.023.
[16] B. Almassri, A. Kreit, F.A. Mahmoud, R. François, Mechanical behaviour of corroded RC beams strengthened by NSM CFRP rods, Compos. B Eng. 64 (2014) 97–107, https://doi.org/10.1016/j.compositesb.2014.04.012.
[17] L. Su, J. Cai, Q. Chen, G. Li, J. Zhao, Investigation on the flexural behavior of corroded concrete beams repaired by CFRP sheet under different corrosion levels, Open Civil Eng. J. 10 (2016) 598–614, https://doi.org/10.2174/1874149501610010598.
[18] R.H. Haddad, Hybrid repair configurations with CFRP composites for recovering structural performance of steel-corroded beams, Constr. Build. Mater. 124 (2016) 508–518, https://doi.org/10.1016/j.conbuildmat.2016.07.124.
[19] M. Elghazy, A. El Refai, U. Ebead, A. Nanni, Effect of corrosion damage on the flexural performance of RC beams strengthened with FRCM composites, Compos. Struct. 180 (2017) 994–1006, https://doi.org/10.1016/j.compstruct.2017.08.069.
[20] A. Siad, M. Bencheikh, L. Hussein, Effect of combined pre-cracking and corrosion on the method of repair of concrete beams, Constr. Build. Mater. 132 (2017) 462–469, https://doi.org/10.1016/j.conbuildmat.2016.12.020.
[21] G.G. Triantafyllou, T.C. Rousakis, A.I. Karabinis, Effect of patch repair and strengthening with EBR and NSM CFRP laminates for RC beams with low,

medium and heavy corrosion, Compos. B Eng. 133 (2018) 101–111, https://doi.org/10.1016/j.compositesb.2017.09.029.
[22] X. Liu, Y. Li, Static bearing capacity of partially corrosion-damaged reinforced concrete structures strengthened with PET FRP composites, Constr. Build. Mater. 211 (2019) 33–43, https://doi.org/10.1016/j.conbuildmat.2019.03.218.
[23] A.H. Al-Saidy, H. Saadatmanesh, S. El-Gamal, K.S. Al-Jabri, B.M. Waris, Structural behavior of corroded RC beams with/without stirrups repaired with CFRP sheets, Mater. Struct. /Materiaux et Constructions. 49 (2016) 3733–3747, https://doi.org/10.1617/s11527-015-0751-y.
[24] B. Fu, X.T. Tang, L.J. Li, F. Liu, G. Lin, InclinedFRP U-jackets for enhancing structural performance of FRP-plated RC beams suffering from IC debonding, Compos. Struct. 200 (2018) 36–46, https://doi.org/10.1016/j.compstruct.2018.05.074.
[25] G. Malumbela, M. Alexander, P. Moyo, Serviceability of corrosion-affected RC beams after patch repairs and FRPs under load, Mater. Struct. /Materiaux et Constructions. 44 (2011) 331–349, https://doi.org/10.1617/s11527-010-9630-8.
[26] G.G. Triantafyllou, T.C. Rousakis, A.I. Karabinis, Corroded RC beams patch repaired and strengthened in flexure with fiber-reinforced polymer laminates, Compos. B Eng. 112 (2017) 125–136, https://doi.org/10.1016/j.compositesb.2016.12.032.
[27] R.H. Haddad, Hybrid repair configurations with CFRP composites for recovering structural performance of steel-corroded beams, Constr. Build. Mater. 124 (2016) 508–518, https://doi.org/10.1016/j.conbuildmat.2016.07.124.
[28] M. Tahershamsi, I. Fernandez, K. Lundgren, K. Zandi, Investigating correlations between crack width, corrosion level and anchorage capacity, Struct. Infrastruct. Eng. 13 (2017) 1294–1307, https://doi.org/10.1080/15732479.2016.1263673.
[29] G. Triantafyllou, T. Rousakis, A. Karabinis, Corroded RC beams at service load before and after patch repair and strengthening with NSM CFRP strips, Buildings. 9 (2019) 67, https://doi.org/10.3390/buildings9030067.
[30] H. Lin, Y. Zhao, P. Feng, H. Ye, J. Ozbolt, C. Jiang, J.-Q. Yang, State-of-the-art review on the bond properties of corroded reinforcing steel bar, Constr. Build. Mater. 213 (2019) 216–233, https://doi.org/10.1016/j.conbuildmat.2019.04.077.
[31] D. Coronelli, K.Z. Hanjari, K. Lundgren, Severely corroded RC with cover cracking, J. Struct. Eng. 139 (2013) 221–232, https://doi.org/10.1061/(ASCE)ST.1943-541X.0000633.
[32] C.G. Berrocal, I. Fernandez, K. Lundgren, I. Löfgren, Corrosion-induced cracking and bond behaviour of corroded reinforcement bars in SFRC, Compos. B Eng. 113 (2017) 123–137, https://doi.org/10.1016/j.compositesb.2017.01.020.
[33] CEN, SS-EN 1504-10:2017 Products and systems for the protection and repair of concrete structures - Definitions, requirements, quality control and evaluation of conformity - Part 10: Site application of products and systems and quality control of the works, SIS, Brussels, 2017. /en/produkter/standardization/vocabularies/construction-materials-and-building-vocabularies/ss-en-1504-102017/ (accessed December 12, 2020).
[34] CEN, SS-EN 12390-3:2019 Testing hardened concrete - Part 3: Compressive strength of test specimens, Brussels, 2019. https://standards.iteh.ai/catalog/standards/cen/7eb738ef-44af-436c-ab8e-e6561571302c/en-12390-3-2019 (accessed November 2, 2020).
[35] CEN, SS-EN 12390-13:2013 Testing hardened concrete - Part 13: Determination of secant modulus of elasticity in compression, Brussels, 2013. /en/produkter/construction-materials-and-building/construction-materials/concrete-and-concrete-products/ssen12390132013/ (accessed December 16, 2020).
[36] I. Lövgren, J.F. Olesen, M. Flansbjer, Application of WST-method for fracture testing of fibre-reinforced concrete, Chalmers University of Technology, Gothenburg, Sweden, 2004, https://research.chalmers.se/en/publication/9239 (accessed November 13, 2020).
[37] ASTM International, A615/A615M-20 Standard Specification for Deformed and Plain Carbon-Steel Bars for Concrete Reinforcement, ASTM International, West Conshohocken, PA, 2020, https://doi.org/10.1520/A0615_A0615M-20 (accessed January 19, 2020).
[38] ASTM International, ASTM D638-14 Standard Test Method for Tensile Properties of Plastics, ASTM International, West Conshohocken, PA, 2014, https://doi.org/10.1520/D0638-14 (accessed November 13, 2020).
[39] J. Yang, R. Haghani, M. Al-Emrani, Innovative prestressing method for externally bonded CFRP laminates without mechanical anchorage, Eng. Struct. 197 (2019), https://doi.org/10.1016/j.engstruct.2019.109416.
[40] ASTM International, ASTM D3039 / D3039M-17 Standard Test Method for Tensile Properties of Polymer Matrix Composite Materials, ASTM International, West Conshohocken, PA, 2017, https://doi.org/10.1520/D3039_D3039M-17.
[41] M. Heshmati, R. Haghani, M. Al-Emrani, Durability of bonded FRP-to-steel joints: effects of moisture, de-icing salt solution, temperature and FRP type, Compos. B Eng. 119 (2017) 153–167, https://doi.org/10.1016/j.compositesb.2017.03.049.
[42] GOM GmbH, ARAMIS Adjustable, (n.d.), https://www.gom.com/metrology-systems/aramis/aramis-adjustable.html (accessed November 13, 2020).
[43] GOM GmbH, GOM Correlate, (n.d.), https://www.gom.com/3d-software/gom-correlate.html (accessed November 13, 2020).
[44] I. Fernandez, K. Lundgren, K. Zandi, Evaluation of corrosion level of naturally corroded bars using different cleaning methods, computed tomography, and 3D optical scanning, Mater Struct. 51 (2018) 78, https://doi.org/10.1617/s11527-018-1206-z.
[45] M. Motavalli, C. Czaderski, K. Pfyl-Lang, Prestressed CFRP for strengthening of reinforced concrete structures: recent developments at Empa Switzerland, J. Compos. Constr. 15 (2011) 194–205, https://doi.org/10.1061/(ASCE)CC.1943-5614.0000125.